Energetic Pulses in Exciton-Phonon Molecular Chains, and Conservative Numerical Methods for Quasi-linear Hamiltonian Systems[*]

Brenton LeMesurier

Department of Mathematics, College of Charleston, South Carolina[†]

(Dated: August 3, 2013)

The phenomenon of coherent energetic pulse propagation in exciton-phonon molecular chains such as α-helix protein is studied using an ODE system model of Davydov-Scott type, both with numerical studies using a new unconditionally stable fourth order accurate energy-momentum conserving time discretization, and with analytical explanation of the main numerical observations.

Impulsive initial data associated with initial excitation of a single amide-I vibration by the energy released by ATP hydrolysis are used, and the best current estimates of physical parameter values. In contrast to previous studies based on a proposed long wave approximation by the nonlinear Schrödinger (NLS) equation and focusing on initial data resembling the soliton solutions of that equation, the results here instead lead to approximation by the third derivative nonlinear Schrödinger equation, giving a far better fit to observed behavior. A good part of the behavior is indeed explained well by the linear part of that equation, the Airy PDE, while other significant features do not fit any PDE approximation, but are instead explained well by a linearized analysis of the ODE system.

A convenient method is described for construction the highly stable, accurate conservative time discretizations used, with proof of its desirable properties for a large class of Hamiltonian systems, including a variety of molecular models.

I. INTRODUCTION

Exciton-phonon systems of ODEs are used to model a variety of molecules in which mobile quantum excitations are present along with mechanical degrees of freedom. A. Davydov [1–3] introduced such a model to study energy propagation in α-helix protein, present for example in the myocins, kenesins and actin involved in muscular contraction, in chains up to 2000 amino acid residues long. A modified version of Davydov's original equations, is used here, incorporating changes suggested by A. Scott [4] and by Davydov and A. Zolotariuk in [5, 6]:

$$\mathrm{i}\hbar\frac{d\psi_n}{dt} + J(\psi_{n-3} + \psi_{n+3}) - L(\psi_{n-1} + \psi_{n+1}) = \chi(q_{n+3} - q_n)\psi_n. \tag{1}$$

$$M\frac{d^2q_n}{dt^2} = V'(q_{n+3} - q_n) - V'(q_n - q_{n-3}) + \chi(|\psi_n|^2 - |\psi_{n-3}|^2), \tag{2}$$

This will be called the *Anharmonic Davydov-Scott system.* The anharmonic potential used here is the cubic

$$V(r) = \frac{K}{2}r^2 - \frac{\gamma}{3}r^3, \tag{3}$$

and in fact it will be demonstrated that for the situation studied herein, it is quite adequate to approximate with the harmonic potential $V(r) = \frac{K}{2}r^2$, $K = V''(0)$, as indeed was done by Davydov originally. This leads to the "harmonic" version of the second equation,

$$M\frac{d^2q_n}{dt^2} = K(q_{n-3} - 2q_n + q_{n+3}) + \chi(|\psi_n|^2 - |\psi_{n-3}|^2). \tag{4}$$

Related exciton-phonon systems arise in other molecular models, such as the system

$$\mathrm{i}\hbar\frac{d\psi_n}{dt} + J(\psi_{n-1} + \psi_{n+1}) = \chi(q_{n+1} - q_{n-1})\psi_n, \tag{5}$$

$$M\frac{d^2q_n}{dt^2} = V'(q_{n+1} - q_n) - V'(q_n - q_{n-1}) + \chi(|\psi_{n+1}|^2 - |\psi_{n-1}|^2), \tag{6}$$

used to model the conducting polymer polydiacetylene in [7]. This differs in having two-sided (symmetrical) form of the coupling, and only nearest neighbor interactions, but as should become clear below, the results herein adapt easily to differences such as these.

We will consider in particular pulses in the exciton variables ψ_n that are generated by initial excitation at one end of the chain. It will be seen that the phenomena are well modeled by a *subsonic limit* leading to a *Helically Coupled Discrete Nonlinear Schrödinger equation* [HDNLS]

$$\mathrm{i}\frac{d\psi_n}{dt} + \hat{J}(\psi_{n-3} + \psi_{n+3}) - \hat{L}(\psi_{n-1} + \psi_{n+1}) + 2\kappa|\psi_n|^2\psi_n = 0. \tag{7}$$

Further, an important part (but not all) of the pulse propagation can be described with a new long-wave PDE approximation; not the nonlinear Schrödinger [NLS] model previously proposed by Davydov and considered in numerous subsequent papers, but a *third derivative NLS equation*

$$\frac{\partial\psi}{\partial t} + \frac{\partial^3\psi}{\partial x^3} + 2\mathrm{i}\kappa|\psi|^2\psi = 0, \tag{8}$$

also seen in related work of D. Pelinowsky and V. Rothos [8].

Section II introduces the various mathematical models and their Hamiltonian structures, symmetries and conserved quantities, explaining the successive approximations involved. Section III introduces the accurate, energy and momentum conserving numerical methods used; these are hopefully useful for a wide variety of similar Hamiltonian systems, due to advantages over the symplectic methods often used for such systems. Section IV presents numerical results, including demonstration of the high degree of accuracy of the successive model simplifications, and the inapplicability (for the present choices of initial data) of the NLS approximations used in various previous studies. Section V gives an analytical explanation for many of the phenomena observed, and ends by proposing some ideas for further study.

II. MODELING EXCITON PROPAGATION IN α-HELIX PROTEIN AND OTHER POLYMERS

A. The Anharmonic Davydov-Scott ODE System

The primary mathematical model used here is the above Anharmonic Davydov-Scott system of ODEs (1,2), which modifies Davydov's original ODE model of α-helix protein by adopting a one-sided form for the exciton-phonon coupling (proposed by A. Scott [4] based on the observations of V. Kuprievich and V. Kudritskaya [9]) and using a nonlinear force for the hydrogen bonds (as introduced by A. Davydov and A. Zolotariuk in [6], and resembling the familiar FPU model). The helical structure of this protein has roughly three amino acid residues per twist, with hydrogen bonds connecting third-nearest neighbors into nearly straight *spines*: spatial proximity leads to attractive exciton coupling along spines in addition to repulsive coupling between neighbors along the molecular backbone being the two dominant exciton interactions.

We briefly summarize the derivation of the above model: see [3–5] for more details. First, one introduces the Hamiltonian operator $\hat{\mathcal{H}} = \hat{\mathcal{H}}_{ex} + \hat{\mathcal{H}}_{ph} + \hat{\mathcal{H}}_{int}$, where:

- The exciton Hamiltonian operator

$$\hat{\mathcal{H}}_{ex} = E_0 \hat{a}_n^\dagger \hat{a}_n - J(\hat{a}_{n+3}^\dagger \hat{a}_n + \hat{a}_{n+3} \hat{a}_n^\dagger) + L(\hat{a}_{n+1}^\dagger \hat{a}_n + \hat{a}_{n+1} \hat{a}_n^\dagger),$$

  describes the amide-I vibrational modes in the residues, with $\hat{a}_n^\dagger$ the creation operator for the vibrational mode in residue n, J the strength of the (attractive) dipole interaction between residues that are adjacent along a spine, L the strength of the (repulsive) dipole interaction between residues that are adjacent along the molecular backbone, and E_0 the total vibrational energy.

- The phonon operator

$$\hat{\mathcal{H}}_{ph} = \sum_n \frac{1}{2M} \hat{p}_n^2 + V(\hat{q}_{n+3} - \hat{q}_n),$$

  gives the energy due to displacement $\hat{q}_n$ of residue n from rest position in the direction of the axis of the helix (that is, along spines), with $\hat{p}_n$ the momentum operator canonically conjugate to $\hat{q}_n$. (More precisely, the energy depends on stretching of the hydrogen bonds.)

- The interaction Hamiltonian operator

$$\hat{\mathcal{H}}_{int} = \chi \sum (\hat{q}_{n+3} - \hat{q}_n) \hat{a}_n^\dagger \hat{a}_n$$

  characterizes the interaction between molecular excitations and displacements, again manifested only through stretching of the hydrogen bonds.

Then seeking solutions of the form

$$|\psi\rangle = \sum_n \psi_n(t) e^{\hat{\sigma}(t)} \hat{a}_n^\dagger |0\rangle,$$

where

$$\hat{\sigma}(t) = \frac{i}{\hbar} \sum_n \left[E_0 t + p_n(t) \hat{q}_n - q_n(t) \hat{p}_n \right],$$

through minimization of $\langle \psi | \hat{\mathcal{H}} | \psi \rangle$ leads to the above Anharmonic Davydov-Scott system of ordinary differential equations, with $\psi_n(t)$ giving the probability of excitation at residue n, and

$$q_n(t) = \langle \psi | \hat{q}_n | \psi \rangle, \quad p_n(t) = \langle \psi | \hat{p}_n | \psi \rangle.$$

These ODE's have the Hamiltonian form

$$i\hbar \frac{d\psi_n}{dt} = \frac{\partial \mathcal{H}}{\partial \psi_n^*}, \quad i\hbar \frac{d\psi_n^*}{dt} = -\frac{\partial \mathcal{H}}{\partial \psi_n}, \tag{9}$$

$$\frac{dq_n}{dt} = \frac{\partial \mathcal{H}}{\partial p_n}, \quad \frac{dp_n}{dt} = -\frac{\partial \mathcal{H}}{\partial q_n}, \tag{10}$$

$$\mathcal{H} = \mathcal{H}_{ex} + \mathcal{H}_{ph} + \mathcal{H}_{int}$$

$$= \sum_n -J(\psi_n^* \psi_{n+3} + \psi_{n+3}^* \psi_n) + L(\psi_n^* \psi_{n+1} + \psi_{n+1}^* \psi_n)$$

$$+ \sum_n \frac{p_n^2}{2M} + V(q_{n+3} - q_n) + \chi \sum_n (q_{n+3} - q_n)\psi_n^* \psi_n. \tag{11}$$

Initial Data. The initial data considered will be for the case of excitation caused by the energy released in a single ATP hydrolysis event: initial excitation at one residue n_0, so that $\psi_n(0) = \delta_{n,n_0}$.

The most interesting phenomena will be seen to arise from excitation at one end of the chain, i.e. $n_0 = 1$, so that

$$\psi_1(0) = 1, \psi_n(0) = 0 \text{ for } n > 1. \tag{12}$$

Note however that ATP hydrolysis can possibly excite two vibrational modes [4, 10] and some numerical studies [4, 11] have used the exciton variables to describe double excitations with initial data $\psi_1(0) = \psi_2(0) = 1$, $\psi_n(0) = 0$ for $n > 2$.

An initially "at rest" chain is used: $q_n(0) = p_n(0) = 0$.

Parameter Values. As the results herein are quite robust under variations in the parameter values within the likely range for α-helix protein, it is for the most part sufficient to use the values reported in [4, 11], which facilitates comparisons to numerous other publications that use those values.

The exciton couplings are best expressed through the frequencies

$$\hat{J} = J/\hbar \approx 1.47 \text{ THz}, \ \hat{L} = J/\hbar \approx 2.33 \text{ THz}.$$

The linear stiffness of the hydrogen bond is $K \approx 13$ N/m. The effective residue mass M is less precisely known, due in part to potential dependence on the particular sequence of amino acids, but it is sufficient to use the typical value $M \approx 0.127$ zg, which leads to a typical phonon frequency

$$\omega_0 = \sqrt{K/M} \approx 10.1 \text{ THz},$$

because it will be seen that the only importance here is that this frequency is substantially larger than the above exciton frequencies. This puts us in the *subsonic* regime: exciton pulses travel at distinctly lower speeds than the phonons. As a further consequence, it will be seen in Section IV that the *subsonic limit* $M \to 0$ (so also $\omega_0 \to \infty$) gives the above HDNLS equation (7), and this approximation is seen in numerical studies to be highly accurate for any physically relevant value of M.

Variation of the interaction coefficient χ has somewhat more significant effects, and despite the precise computed value of 34 pN cited by [11] and various subsequent papers, there is still substantial uncertainty as to its value: the best current estimate appears to be the broad range of experimental values $\chi \approx 35-62$ pN, with computed values subject to far greater uncertainty, even as to its sign [10]. Thus the effect of varying this parameter is studied below: fortunately, it is seen that the results herein depend only mildly on this value, with even the linearization $\chi = 0$ giving useful information.

Boundary Conditions. The boundary conditions at the ends of the chain depend on if and how the helix is connected to other parts of a molecule, but here the simplest, unbound form is assumed: "out of bounds" values of ψ_n and of the *bond-stretchings* $r_n := q_{n+3} - q_n$ are effectively neglected in the Hamiltonian, so for such index values

$$\psi_n = 0, \ r_n = 0. \tag{13}$$

For constructing simplified PDE models via a long wave approximation, it is also convenient to consider an infinite chain with $n \in \mathbb{N}$ and $\psi_n \to 0$, $r_n \to 0$ as $|n| \to \infty$.

B. Momenta (conserved quantities other than the Hamiltonian)

The equations above have a conserved *exciton number* $\mathcal{E} = \sum_n \psi_n^* \psi_n$, with the initial data of interest here giving $\mathcal{E} = 1$. (See however the note above about previous papers that model double excitations and thus have $\mathcal{E} = 2$.) This invariant is associated via Noether's Theorem with a linear symmetry group action, the gauge symmetry

$$\psi_n \to e^{is}\psi_n, \ \psi_n^* \to e^{-is}\psi_n^*. \tag{14}$$

There is also a conserved momentum $\mathcal{P}_\sigma$ on each spine, $\mathcal{P}_\sigma = \sum_m p_{3m+\sigma}$, associated with spine translation symmetries $q_{3m+\sigma} \to q_{3m+\sigma} + s_\sigma$. However, linear invariants like this are exactly conserved by almost any reasonable time discretization (for example, any Runge-Kutta method) so no more will be said about this.

C. Approximation by a Helically Coupled Nonlinear Schrödinger Equation

The Davydov-Scott system has several disparate scales in both space and time, and these can be used to derive simpler approximations.

The first is that for physically relevant initial data, it will be seen in the numerical results of Section IV that the bond-stretchings r_n are of small enough amplitude that the linearized force $-Kr$ is an adequate approximation, corresponding to harmonic potential $V(r) = \frac{K}{2}r^2$.

Next is the *subsonic limit* approximation: the frequency ω_0 is considerably higher than the exciton coupling frequencies $\hat{J}$ and $\hat{L}$, so that variation in the amplitude $|\psi_n|$ is far slower that that of the mechanical variables q_n. Solving Eq. (4) by variation of parameters gives

$$r_n = q_{n+3} - q_n$$
$$= -\frac{\chi}{K}|\psi_n|^2 + \text{oscillations of characteristic frequency } \omega_0,$$

and it is plausible that the excitons respond primarily to the slowly varying moving average part, which is given by setting $M = 0$ in (4). Using this moving average approximation $r_n \approx -\frac{\chi}{K}|\psi_n|^2$ in the exciton equation (1) eliminates the mechanical variables, reducing the model to the *Helically Coupled Discrete Nonlinear Schrödinger [HDNLS] equation* (7), with

$$\kappa := \frac{\chi^2}{2\hbar K} \approx 0.45 - 1.4 \text{ THz.}$$

This has Hamiltonian

$$\mathcal{H} = \sum_n - J(\psi_n^*\psi_{n+3} + \psi_{n+3}^*\psi_n) + L(\psi_n^*\psi_{n+1} + \psi_{n+1}^*\psi_n)$$
$$- \kappa(\psi_n^*\psi_n)^2. \tag{15}$$

The validity of this approximation is demonstrated numerically in Section IV.

III. ENERGY-MOMENTUM CONSERVING TIME DISCRETIZATIONS

To study these systems and assess the adequacy of the above HDNLS approximation, some numerical solutions should be considered. For that, the necessary numerical methods will now be described, and this is done for a general Hamiltonian system

$$\frac{d\mathbf{y}}{dt} = \mathcal{J}\nabla_\mathbf{y}\mathcal{H}(\mathbf{y}) = \mathcal{J}\frac{\partial\mathcal{H}}{\partial\mathbf{y}}(\mathbf{y}) \tag{16}$$

with $\mathcal{J}$ an anti-symmetric matrix.

Notation. For the time step from t to $t+\delta t$ and any scalar variable y or vector $\mathbf{y}$, we use the variable's name alone to denote its value at time t, $t^+ = t + \delta t$, $y^+ = y(t^+) = y(t+\delta t)$, $\delta y = y^+ - y$, and $\bar{y} = \frac{y + y^+}{2}$.

A. Discrete Gradient Methods for Exact Energy Conservation

Exact conservation of invariants has been seen to be a desirable feature of numerical methods for Hamiltonian systems; see for example [12]. Following ideas originating in the work of O. Gonzalez and J. Simo [13, 14], the first step is to ensure conservation of the Hamiltonian (energy) by approximating such a system by a *discrete Hamiltonian system*

$$\frac{\delta\mathbf{y}}{\delta t} = \mathcal{J}\tilde{\nabla}_\mathbf{y}\mathcal{H}(\mathbf{y}, \mathbf{y}^+) \tag{17}$$

using a suitable *discrete gradient* approximation

$$\tilde{\nabla}_\mathbf{y}f(\mathbf{y}, \mathbf{y}^+) \approx \nabla_\mathbf{y}f(\mathbf{y}) \tag{18}$$

that satisfies the *Discrete Chain Rule*

$$\delta f = (\tilde{\nabla}_{\mathbf{y}} f)(\mathbf{y}, \mathbf{y}^+) \cdot \delta \mathbf{y}. \tag{19}$$

This condition is assumed from now on, along with linearity and the consistency condition

$$\lim_{\mathbf{y}^+ \to \mathbf{y}} (\tilde{\nabla}_{\mathbf{y}} f)(\mathbf{y}, \mathbf{y}^+) = \nabla_{\mathbf{y}} f(\mathbf{y}). \tag{20}$$

Component notation like

$$\tilde{\nabla}_{\mathbf{y}} f(\mathbf{y}, \mathbf{y}^+) = \left\langle \tilde{D}_{y_1} f(\mathbf{y}, \mathbf{y}^+), \ldots \right\rangle$$

will occasionally be used.

Conservation of energy is easily shown for a discrete gradient method by mimicking the familiar argument for (continuous) Hamiltonian systems: using in succession (19), (17), and the anti-symmetry of $\mathcal{J}$,

$$\begin{aligned}
\frac{\delta \mathcal{H}}{\delta t} &= (\tilde{\nabla}_{\mathbf{y}} \mathcal{H})(\mathbf{y}, \mathbf{y}^+) \cdot \frac{\delta \mathbf{y}}{\delta t} \\
&= (\tilde{\nabla}_{\mathbf{y}} \mathcal{H})(\mathbf{y}, \mathbf{y}^+) \cdot \mathcal{J}(\tilde{\nabla}_{\mathbf{y}} \mathcal{H})(\mathbf{y}, \mathbf{y}^+) = 0.
\end{aligned}$$

B. Choosing a Discrete Gradient that Also Respects Quadratic Momenta

Many such "energy conserving" discrete gradients can be found, but conserving other invariants (here all called *momenta*) requires an appropriate choice of the gradient approximation. It will be seen that there is a natural limitation to quadratic (including linear) momenta, but this is sufficient for most systems of physical relevance. Here the approach introduced in [15, 16] is followed, which is based on three facts:

1. There is a unique discrete gradient for functions of a single variable y

$$\tilde{\nabla}_y f(y, y^+) := \begin{cases} \dfrac{\delta f}{\delta y}, & y^+ \neq y \\[2mm] \dfrac{df}{dy}(y), & y^+ = y \end{cases} \tag{21}$$

following from the chain rule requirement (19). For polynomials, this simplifies in a way that avoids the division by zero issue, via

$$\tilde{\nabla}_y y^{p+1} = y^n + y^{n-1} y^+ + \cdots + (y^+)^n. \tag{22}$$

2. There is a unique time-reversal symmetric discrete gradient for a product of two variables

$$\delta(y_j y_k) = \overline{y}_j \delta y_k + \overline{y}_k \delta y_j \tag{23}$$

which corresponds to evaluating the true gradient at the midpoint:

$$\tilde{\nabla}(y_j y_k)(\mathbf{y}, \mathbf{y}^+) = \nabla(y_j y_k)(\overline{\mathbf{y}}). \tag{24}$$

In fact this extends to a *discrete product rule* based on

$$\delta(fg) = \overline{f} \delta g + \overline{g} \delta f. \tag{25}$$

Thus linear terms in the equations, corresponding to quadratic terms in the Hamiltonian, are discretized exactly as for the implicit midpoint rule, which is a popular momentum conserving symplectic method for Hamiltonian systems. The only differences are for nonlinearities, which for the systems of interest herein are those coming from the Hamiltonian terms

$$\begin{aligned}
&\chi(q_{n+3} - q_n)\psi_n^* \psi_n \quad \text{and} \\
&\frac{\gamma}{3}(q_{n+3} - q_n)^3 \quad \text{for Eq's (1,2)}; \\
&\kappa(\psi_n^* \psi_n)^2 \quad \text{for Eq. (7)}.
\end{aligned} \tag{26}$$

3. Many physically relevant Hamiltonian systems with conserved momenta have a natural form in which all the momenta are quadratic (including linear) functions of the state variables, and are related through Noether's theorem to a group of affine symmetries of the Hamiltonian $\mathcal{H}$, with invariance of $\mathcal{H}$ manifested by the fact that it can be expressed as a composition

$$\mathcal{H}(\mathbf{y}) = \hat{\mathcal{H}}(\mathbf{Q}), \tag{27}$$

where each component Q_m of the new state vector $\mathbf{Q}$ is a quadratic

$$Q_m = \frac{1}{2} \sum_{j,k} A_m^{jk} y_j y_k + \sum_j b_m^j y_j \tag{28}$$

(with each $A_m := \{A_m^{jk}\}$ symmetric) that is invariant under the symmetry group. For example, with the systems seen herein, the invariant quadratics with which the Hamiltonian can be expressed are the exciton products $e_{n,m} = \psi_n^* \psi_m$ and the bond-stretchings r_n.

In particular, the nonlinear terms seen here are

$$\chi r_n e_{n,n}, \ \frac{\gamma}{3} r_n^3, \ \text{and} \ \kappa e_{n,n}^2. \tag{29}$$

The discrete Jacobian of this change of variables is given by the true Jacobian evaluated at the midpoint:

$$\tilde{D}_{\mathbf{y}} \mathbf{Q}(\mathbf{y}, \mathbf{y}^+) = D_{\mathbf{y}} \mathbf{Q}(\bar{\mathbf{y}}).$$

These facts and the above chain rule requirement naturally lead to:

$$\begin{aligned} \tilde{\nabla}_{\mathbf{y}} \mathcal{H} &= \sum_m \tilde{D}_m \hat{\mathcal{H}}(\mathbf{Q}, \mathbf{Q}^+) \, \tilde{\nabla}_{\mathbf{y}} Q_m(\mathbf{y}, \mathbf{y}^+), \\ &= \sum_m \tilde{D}_m \hat{\mathcal{H}}(\mathbf{Q}, \mathbf{Q}^+) \, \nabla_{\mathbf{y}} Q_m(\bar{\mathbf{y}}). \end{aligned} \tag{30}$$

For the nonlinearities herein, the discrete gradients are now determined by the factorizations in (29) through simple forms:

$$\begin{aligned} \tilde{D}_r(re) &= \bar{e}, \ \tilde{D}_e(re) = \bar{r}, \\ \tilde{D}_e(e^2) &= 2\bar{e}, \ \tilde{D}_r(r^3) = r^2 + rr^+ + (r^+)^2, \end{aligned} \tag{31}$$

using (22) for the last.

Using such a discrete gradient, energy and momenta will be conserved with any choice for the factors $\tilde{D}_m \hat{\mathcal{H}}(\mathbf{Q}, \mathbf{Q}^+)$. In practice, the above rules for single variable functions, products, compositions, and linearity are generally enough to construct a suitable discrete gradient for $\hat{\mathcal{H}}$.

Theorem 1 *For a Hamiltonian system*

$$\frac{d\mathbf{y}}{dt} = \mathcal{J} \nabla_{\mathbf{y}} \mathcal{H}(\mathbf{y}), \quad \mathcal{H}(\mathbf{y}) = \hat{\mathcal{H}}(\mathbf{Q})$$

as described above, and thus with a discrete gradient

$$\tilde{\nabla}_{\mathbf{y}} \mathcal{H} = \sum_m \tilde{D}_m \hat{\mathcal{H}}(\mathbf{Q}, \mathbf{Q}^+) \, \nabla_{\mathbf{y}} Q_m(\bar{\mathbf{y}}),$$

solving numerically by the corresponding discrete gradient method

$$\frac{\mathbf{y}^+ - \mathbf{y}}{\delta t} = \mathcal{J} \sum_m \tilde{D}_m \hat{\mathcal{H}}(\mathbf{Q}, \mathbf{Q}^+) \, \nabla_{\mathbf{y}} Q_m \left(\frac{\mathbf{y} + \mathbf{y}^+}{2} \right) \tag{32}$$

conserves the Hamiltonian and all the quadratic momenta.

Proof of Theorem 1 Energy conservation is already established above, so consider conservation of an invariant Q. Such quadratics are in fact invariant for any Hamiltonian $\mathcal{H} = \hat{\mathcal{H}}(\mathbf{Q})$ constructed from the quadratic forms Q_m as in (27), including the alternative choices $\mathcal{H}_m := Q_m$, and invariance of Q on each of those Hamiltonian flows means that

$$0 = \frac{dQ}{dt} = \nabla Q \cdot \mathcal{J} \nabla \mathcal{H}_m = \nabla Q \cdot \mathcal{J} \nabla Q_m, \tag{33}$$

so that we have vanishing of the Poisson brackets

$$\{Q, Q_m\}(\mathbf{y}) := \nabla Q(\mathbf{y}) \cdot \mathcal{J} \nabla Q_m(\mathbf{y}) = 0. \tag{34}$$

Mimicking (33) for the discrete flow and using the fact from (24) that discrete gradients of quadratics are given by the true gradients at the midpoint gives

$$\frac{\delta Q}{\delta t} = \tilde{\nabla} Q \cdot \mathcal{J} \tilde{\nabla} \mathcal{H} = \nabla Q(\overline{\mathbf{y}}) \cdot \mathcal{J} \sum_m (\tilde{D}_m \hat{\mathcal{H}}) \nabla Q_m(\overline{\mathbf{y}})$$

$$= \sum_m (\tilde{D}_m \hat{\mathcal{H}}(\mathbf{Q}, \mathbf{Q}^+)) \{Q, Q_m\}(\overline{\mathbf{y}}).$$

Evaluating (34) at $\mathbf{y} = \overline{\mathbf{y}}$ gives $\{Q, Q_m\}(\overline{\mathbf{y}}) = 0$, so $\delta Q = 0$.

C. Practical Implementation: an Iterative Solution Method

The system of equations will be nonlinear (unless the Hamiltonian system itself is linear), so we need an iterative solution method. To exploit the quasi-linearity of the system to preserve linear stability properties and exact momentum conservation without the cost of a full quasi-Newton method, we proceed as follows: construct successive approximations $\mathbf{y}^{(k)}$ of $\mathbf{y}^+$ by solving

$$\frac{\mathbf{y}^{(k)} - \mathbf{y}}{\delta t} = \mathcal{J} \sum_m \tilde{D}_m \hat{\mathcal{H}}(\mathbf{Q}, \mathbf{Q}^{(k-1)}) \, \nabla_{\mathbf{y}} Q_m(\overline{\mathbf{y}}^{(k)}), \tag{35}$$

where $\overline{\mathbf{y}}^{(k)} = (\mathbf{y} + \mathbf{y}^{(k)})/2$ and $\mathbf{Q}^{(k-1)} = \mathbf{Q}(\mathbf{y}^{(k-1)})$, and initialization can be with $\mathbf{y}^{(0)} = \mathbf{y}$ or some other suitable approximation of $\mathbf{y}^+$.

That is, the nonlinear part $\tilde{\nabla}_{\mathbf{Q}} \hat{\mathcal{H}}$ is approximated using the current best available approximation $\mathbf{y}^{(k-1)}$ of $\mathbf{y}^+$, while the linear terms are left in terms of the unknown $\mathbf{y}^{(k)}$ to be solved for. This equation is linear in the unknown $\mathbf{y}^{(k)}$, making its solution straightforward, particularly with the narrow coupling bandwidth in the systems studied here. Much as above, we have:

Theorem 2 *Each iterate $\mathbf{y}^{(k)}$ given by the above scheme (35) conserves all quadratic first integrals that are conserved by the original discrete gradient scheme (32).*

The proof is as for Theorem 1 except that the Poisson brackets are evaluated at $\left(\mathbf{y} + \mathbf{y}^{(k)}\right)/2$.

This approach to iterative solution also gives unconditional linear stability, since as noted above, for a linear system it is the same as the A-stable implicit midpoint method, and indeed only a single iteration is needed in that case. Energy is of course only conserved in the limit $k \to \infty$, but iterating until energy is accurate within machine rounding error is typically practical: if this take too many iterations, it is better for overall accuracy to reduce the time step size δt to speed the convergence.

D. Time Discretization for the Davydov-Scott System

Applying the above results to the anharmonic Davydov-Scott system is mostly a matter of separating linear terms from nonlinear, applying the implicit midpoint rule to the former and using Eq. (31) in Eq. (35) for the latter:

$$i\frac{\delta \psi_n^{(k)}}{\delta t} + \hat{J} \left(\overline{\psi}_{n-3}^{(k)} + \overline{\psi}_{n+3}^{(k)}\right) - \hat{L} \left(\overline{\psi}_{n-1} + \overline{\psi}_{n+1}\right)$$

$$= \frac{\chi}{\hbar} \left(\overline{q}_{n+3}^{(k-1)} - \overline{q}_n^{(k-1)}\right) \overline{\psi}_n^{(k)}, \tag{36}$$

$$M \frac{\delta q_n^{(k)}}{\delta t} = \overline{p}_n^{(k)}, \tag{37}$$

$$
\begin{aligned}
\frac{\delta p_n^{(k)}}{\delta t} = {} & K(\overline{q}_{n+3}^{(k)} - \overline{q}_n^{(k)}) + \chi \left(\overline{|\psi_n^{(k-1)}|^2} - \overline{|\psi_{n-3}^{(k-)}|^2} \right) \\
& - \frac{\gamma}{3} \Bigg[\left(q_{n+3}^{(k-1)} - q_n^{(k-1)} \right)^2 \\
& \quad + \left(q_{n+3}^{(k-1)} - q_n^{(k-1)} \right) \left((q^+)_{n+3}^{(k-1)} - (q^+)_n^{(k-1)} \right) \\
& \quad + \left((q^+)_{n+3}^{(k-1)} - (q^+)_n^{(k-1)} \right)^2 \Bigg].
\end{aligned} \tag{38}
$$

E.   Higher Order Accuracy by Symmetric Step Composition

The methods seen so far are only second order accurate in time. Fortunately, the method of *symmetric step composition*, (developed by M. Creutz, A. Gocksch, E. Forest, M. Suzuki and H. Yoshida [17–20] for use with symplectic methods, and reviewed by E. Hairer, C. Lubich, and G. Wanner in the book [12]) gives a systematic way to construct methods of any higher even order while preserving all the interesting properties: conservation of the Hamiltonian and quadratic invariants, time-reversal symmetry, and unconditional stability.

Numerical results are computed below by combining the above discrete gradient method with the fourth-order accurate Suzuki form of step composition [12, Example II.4.3, p. 45]: compose five discrete gradient steps of lengths $\rho_j \delta$,

$$\rho_1 = \rho_2 = \rho_4 = \rho_5 = \frac{1}{4 - \sqrt[3]{4}} \approx 0.41,$$

$$\rho_3 = 1 - 4\rho_1 \approx -0.66.$$

F.   Comparisons to Other Methods

The most commonly used conservative methods for Hamiltonian systems are symplectic methods, which can conserve momenta but cannot in general conserve energy, as described by a theorem of Z. Ge and J. Marsden [21]. In the present situation with stiff systems of ODEs and Hamiltonian not of purely mechanical form $\mathcal{H}(\mathbf{q}, \mathbf{p}) = K(\mathbf{p}) + U(\mathbf{q})$, the preferred choices of symplectic method are the implicit midpoint method, higher order Diagonally Implicit Runge-Kutta [DIRK] methods, and fully implicit Gaussian Runge-Kutta methods.

All DIRK symplectic methods are cognates of the energy-momentum methods described here, given by applying the same step composition procedures to the implicit midpoint method instead of to the discrete gradient method. It has been illustrated in [15, 16] that the basic discrete gradient method can handle qualitative features of solutions better than the midpoint method, though this has not been tested directly when step composition is applied to each method.

Gaussian symplectic methods can be desirable when the time step size is small enough to allow their solution by simple fixed point iteration, but are not cost effective for stiff systems, where an unconditionally stable iterative method such as that above is highly desirable.

IV.   NUMERICAL RESULTS

As the initial excitation due to ATP hydrolysis will occur at at most two residues, the initial state is very far from the slowly varying form assumed in long wave approximations by PDE's. Thus one question addressed here, as in earlier work like [4, 11], is whether solutions with such initial data evolve into a form that can be well-approximated at later times by a smooth function of position, leading to a hopefully more tractable PDE model.

Time Step Choice.   The choice of time steps here is always cautiously constrained by

$$\delta t \leq \min \left(\frac{1}{2(\hat{J} + \hat{L})}, \frac{1}{\omega_0} \right),$$

which satisfies the natural accuracy and stability requirements for explicit methods, and for convergence of basic fixed point iterative solution of the nonlinear schemes. However it is confirmed that accurate solutions, in the sense that all graphs of exciton data are completely indistinguishable from results with smaller time steps, are given for any time step size

$$\delta t \leq \frac{1}{2(\hat{J} + \hat{L})}$$

depending only on the time scale manifested in the exciton evolution equation. Thus the time discretization is effectively handling any faster time scales in the mechanical variables in the innocuous way that one hopes for stiff modes to be handled by an unconditionally stable method, with no adverse effect on the accuracy of the more slowly evolving (exciton) variables.

A.   Numerical Observations for the Davydov-Scott and HDNLS Systems

We first solve the Anharmonic Davydov-Scott system (1,2) with 1000 residues, hydrogen bond nonlinearity of cubic form (3) with $\gamma = 4$, and initial excitation at one end as in (12). Figure 1 is for $\chi = 35$, the minimum of the likely range cited above, showing the exciton amplitude $|\psi_n|$ at times $t = 20$ and 40. It reveals a dominant leading pulse of speed about 13.3 residues per unit time that is slowly varying in n, and a secondary pulse of speed about 6.4 with no slow spatial variation.

The time evolution is very similar in all cases, so it is sufficient to compare at a single time $t = 40$ from now on. Figure 2 repeats the forward part of the above data at that time, and Figure 3 is the same except for $\chi = 62$, the other extreme of the likely range of values. Although a significant quantitative difference is seen, the qualitative description above still holds for the stronger nonlinearity, and it will be seen soon that other key features are also unchanged.

For the sake of comparison to the somewhat different results of [11], note that those differ in using the two-point initial impulse form $\psi_1(0) = \psi_2(0) = 1$, $\psi_n(0) = 0$ for $n > 2$, $\chi = 40$, $N = 600$, time units of 0.1ps, and the symmetrical exciton-coupling coupling form as seen in the polydiacetylene model of Equations (5,6).

The slow variation of exciton amplitude suggests the possibility of a long wave PDE approximation for this part of the solution, as proposed by Davydov and others. However, slow variation is not seen in ψ_n as a whole, due to rapid phase variation, and this is true even if one restricts to individual spines. Instead, the phase advances by a factor of approximately $-i$ at each step along the chain, and thus by factor of i at each step along a spine. This is best revealed by studying $w_n := i^{n-1}\psi_n$: the real and imaginary parts of this are shown in Figures 3 and 4 for the two cases above.

Next, it can observed that the nonlinearity of the hydrogen bonds is of little significance, due to the magnitude of r_n staying quite small: less than about 0.3. This is indicated by Figure 6 for the harmonic case $\gamma = 0$, with $\chi = 35$.

However, this point is made more emphatically by considering the next level of approximation, by the subsonic limit of HDNLS (7). Even for the harder case of $\chi = 62$, the exciton form is little changed, as seen in Figure 7, and it is much the same over the full range of likely χ values.

B.   The Linear Approximation $\chi \to 0$

A final approximation worth considering is $\chi \to 0$, which for either the Davydov-Scott or HDNLS systems gives a linear equation for the excitons alone:

$$i\frac{d\psi_n}{dt} + \hat{J}(\psi_{n+3} + \psi_{n-3}) - \hat{L}(\psi_{n+1} + \psi_{n-1}) = 0. \tag{39}$$

This will be the starting point for the analysis below, but first it can be observed that at least some main qualitative features of the above solutions are retained in this linear model, as seen in Figures 8 and 9. The form of w_n might now be recognized as resembling the Airy function Ai, and this will be explained in the analysis of the next section.

C.   Brief Remarks on Other Cases

Some brief observations for other choices of initial data and parameter values.

1. For an initial impulse at other locations, one has exciton self-trapping, with most of the signal staying at the initial location. There are weaker pulses propagating in each direction, which are well explained by the analysis of linearized equations given in the next section.
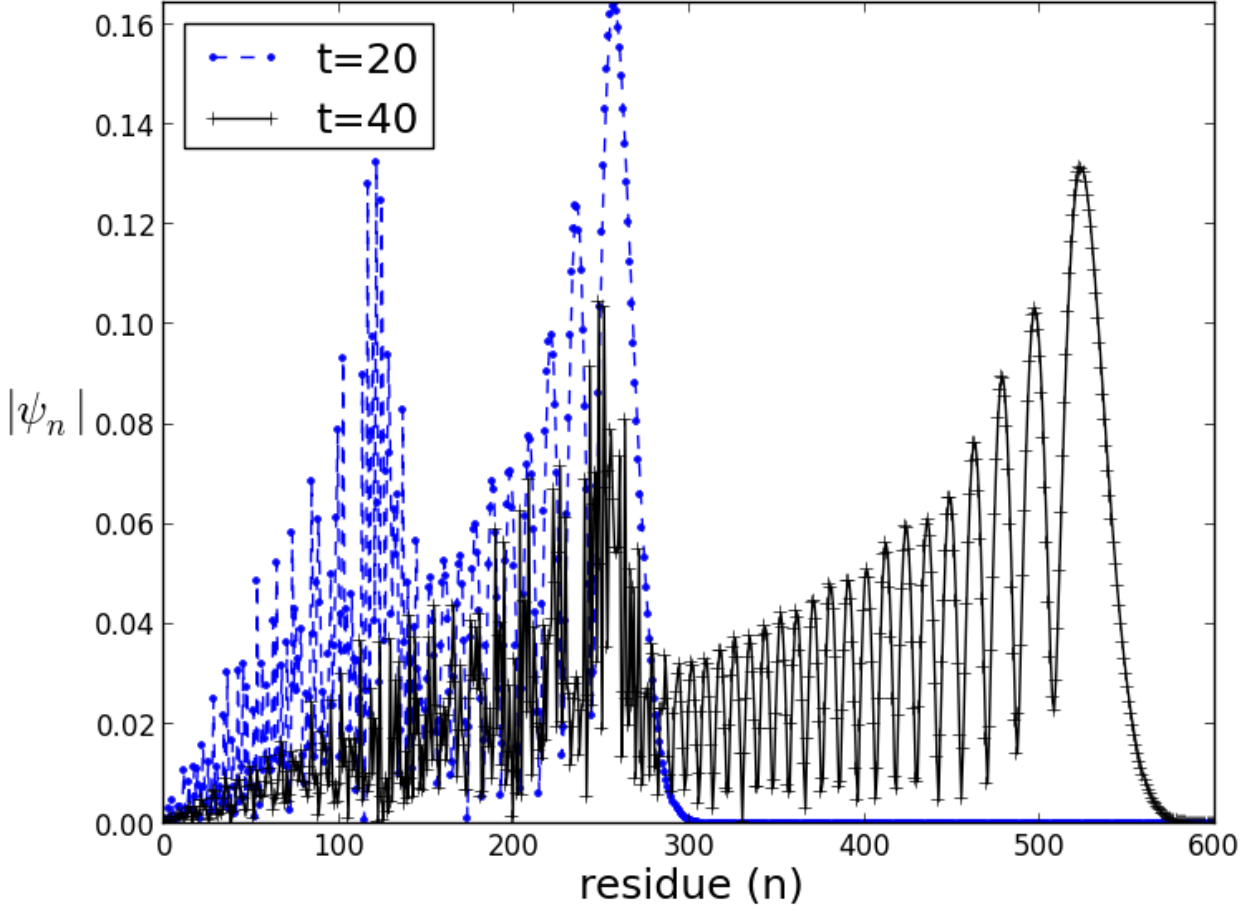
FIG. 1. (Color online) $|\psi_n|$ at times $t = 20, 40$ for the Anharmonic Davydov-Scott system with nonlinear coupling $\chi = 35$, force anharmonicity $\gamma = 4$, and impulsive initial data $\psi_n(0) = \delta_{1n}$ as in Eq. (12).

2. For larger values of χ, about 100 and up, there is again strong exciton self-trapping, with little signal propagation.

3. For the double excitation initial data $\psi_1(0) = \psi_2(0) = 1$, $\psi_n(0) = 0$ for $n > 2$ as considered in [11], or equivalently with normalization $\psi_1(0) = \psi_2(0) = 1/\sqrt{2}$ and χ increased by $\sqrt{2}$ the behavior is similar to that discussed here, though with somewhat stronger nonlinear effects.

4. For a straight-chain exciton-phonon model and/or with symmetric exciton-phonon coupling, both seen in the polydiacetylene model of Equations (5,6), the main phenomena are similar, though removing the third-nearest neighbor coupling changes the pulse velocity and eliminates the slower second pulse.

V.   ANALYSIS, AND THE THIRD DERIVATIVE NLS APPROXIMATION

Previous studies have proposed a PDE approximation based on the assumption that $\psi_n(t)$ varies slowly in n, leading to PDEs related to the nonlinear Schrödinger equation, and thus to the study of solutions related to its traveling wave solutions of hyperbolic secant form. However, it is seen above that for the impulsive initial data considered herein, ψ_n does not become slowly varying in phase. Instead, slow variation along the chain is seen in the transformed quantity
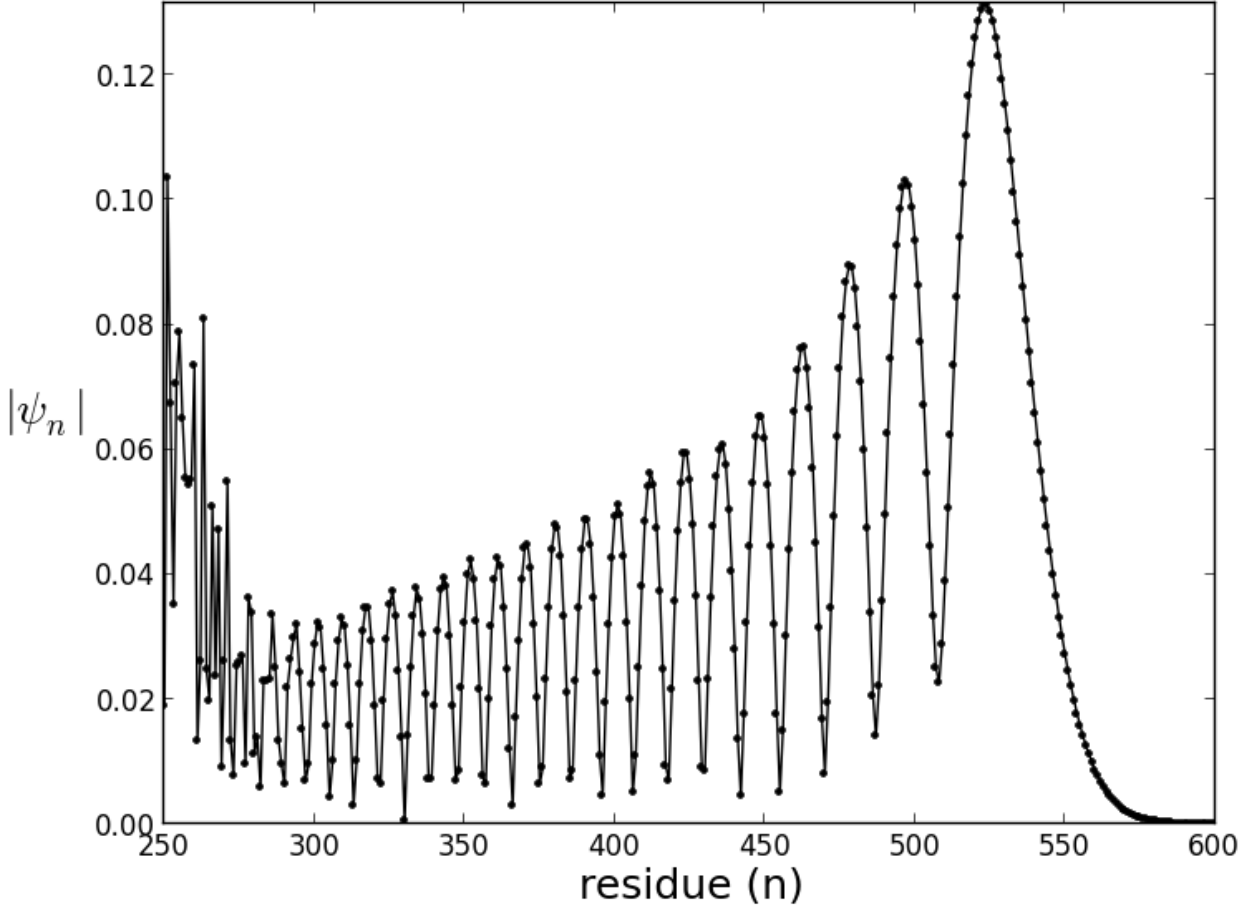
FIG. 2. $|\psi_n|$ for the Anharmonic Davydov-Scott system, as in Fig. 1 except at $t = 40$ only.

$w_n = i^{n-1}\psi_n$, for which the Davydov-Scott exciton evolution equation (2) becomes

$$\frac{dw_n}{dt} + \hat{J}(w_{n+3} - w_{n-3}) + \hat{L}(w_{n+1} - w_{n-1})$$
$$= -i\frac{\chi}{\hbar}(q_{n+3} - q_n)w_n, \tag{40}$$

and HDNLS becomes

$$\frac{dw_n}{dt} + \hat{J}(w_{n+3} - w_{n-3}) + \hat{L}(w_{n+1} - w_{n-1})$$
$$= 2i\kappa|w_n|^2 w_n. \tag{41}$$

Recalling that $\hat{J} \approx 1.47$ THz and $\hat{L} = 2.33$ THz whereas $\kappa \approx 0.45 - 1.4$ THz, and that our initial data ensures $|w_n| \leq 1$ with far smaller values typical, it appears likely that the linearization

$$\frac{dw_n}{dt} + \hat{J}(w_{n+3} - w_{n-3}) + \hat{L}(w_{n+1} - w_{n-1}) = 0 \tag{42}$$

is a useful first approximation.

One initial observation is that for the initial data considered herein, this has real valued solutions, fitting with the observed phase behavior. Following the approach of D. Pelinowsky and V. Rothos [8], we seek solutions of the form

$$\psi_n(t) = e^{i(kn-\omega t)}w(\tau, z), \ z = (n - vt)h, \tau = \epsilon t, h, \epsilon \ll 1 \tag{43}$$
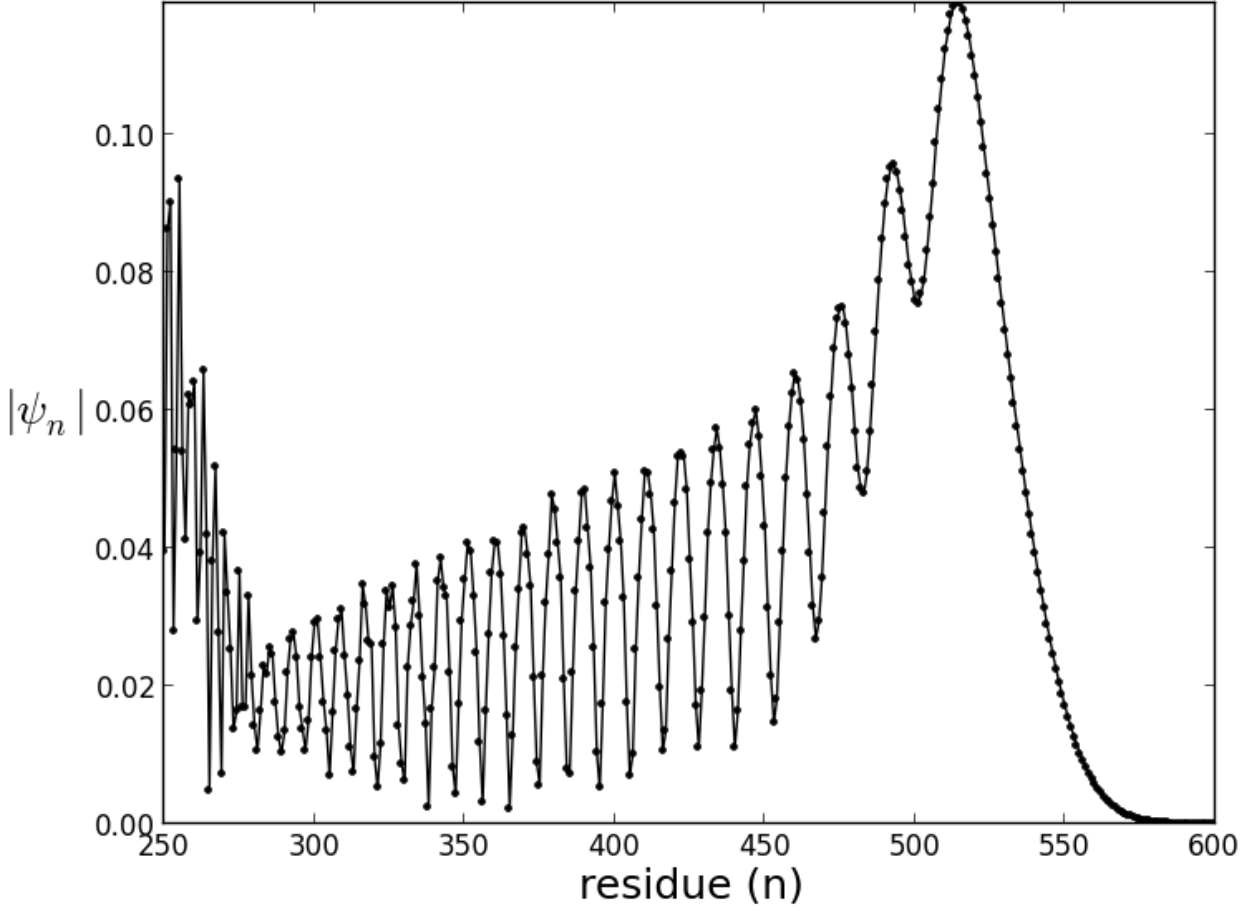
FIG. 3. $|\psi_n|$ at $t = 40$ for the Anharmonic Davydov-Scott system with stronger nonlinear coupling $\chi = 62$, otherwise as in Fig. 2.

where the fast spatial and time scales are isolated in an exponential factor, leaving a slowly varying envelope $w(\tau, z)$. In the limit $\chi \to 0$, we first seek the simple traveling waves of the linearization (39) given by constant w. This has dispersion relation

$$\omega(k) = \hat{J}\cos(3k) - 2\hat{L}\cos(k), \tag{44}$$

and thus group velocity

$$v = \frac{d\omega}{dk} = 6\hat{J}\sin(3k) - 2\hat{L}\sin(k), \tag{45}$$

with maximum

$$v = v_{max} = 6\hat{J} + 2\hat{L} \approx 13.48 \tag{46}$$

occurring for $k = -\pi/2$ and $\omega = 0$. This gives

$$\psi_n = (-\mathrm{i})^{n-1}w, \tag{47}$$

the same transformation suggested above based on numerical observations. (There is a left going counterpart of course, excluded by the initial data used here.)
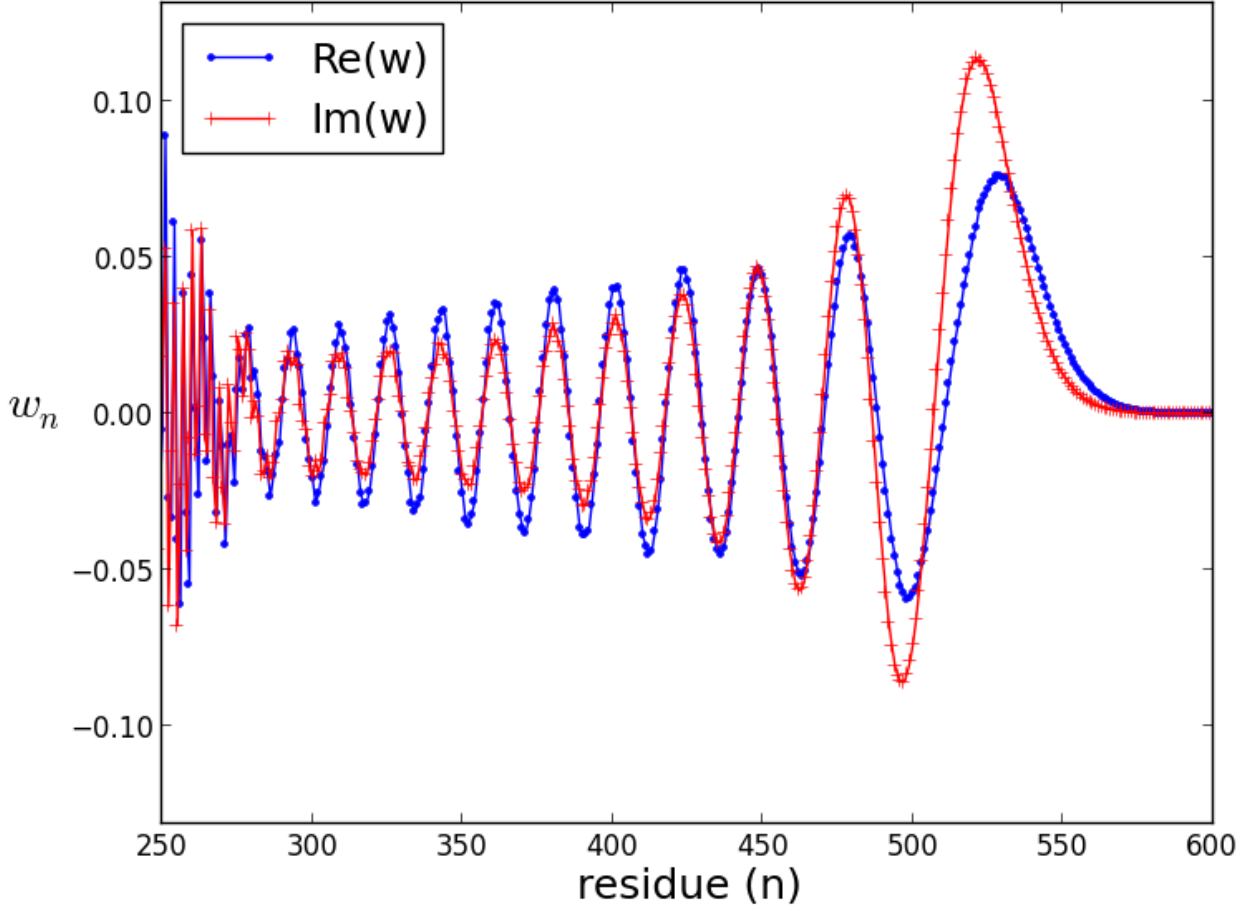
FIG. 4. (Color online) Real and imaginary parts of $w_n = \mathrm{i}^{n-1}\psi_n$ at $t = 40$ for the Davydov system with parameters as in Fig. 2: $\chi = 35$, $\gamma = 4$, impulsive initial data.

One way to see this is that from initially impulsive initial data with a wide range of wave numbers present, there is a clustering of signals of various wave numbers at critical numbers of group velocity, $dv/dk = 0$, in particular at $k = -\pi/2$, which gives the maximum velocity. There are in fact six critical numbers, with the other two that correspond to right-going pulses forming a supplementary pair $k' \approx 0.15\pi$, $k'' = \pi - k'$ with the same velocity $v' \approx 6.60$, fitting well the velocity of about 6.4 observed for the second slower pulse above. This double root allows pulses with spatial dependence given by superposition of the two exponential solutions, with forms that alternate between $\cos(\beta'n)$ and $\mathrm{i}\sin(\beta'n)$ at successive nodes, which explains the break-down of slow amplitude variation seen for that second pulse.

Returning to the Davydov-Scott system, we now seek solutions similar to this. Nonlinearity requires an amplitude scaling, and this is incorporated along with an approximately traveling wave form using the above group velocity in the transformation

$$\psi_n(t) = \mathrm{i}^{n-1}w_n(t) \approx \sqrt{\epsilon}\,\mathrm{i}^n u(z,\tau), \tag{48}$$

where $z = (n - vt)h$, $v = 6\hat{J} + 2\hat{L}$, $\tau = \epsilon t$, $\epsilon = (1/3)ah^3$, $a = 27\hat{J} + \hat{L}$.

This gives

$$u_\tau + u_{zzz} = \mathrm{i}\hat{\chi}q_z u, \tag{49}$$

and in the subsonic limit of HDNLS,

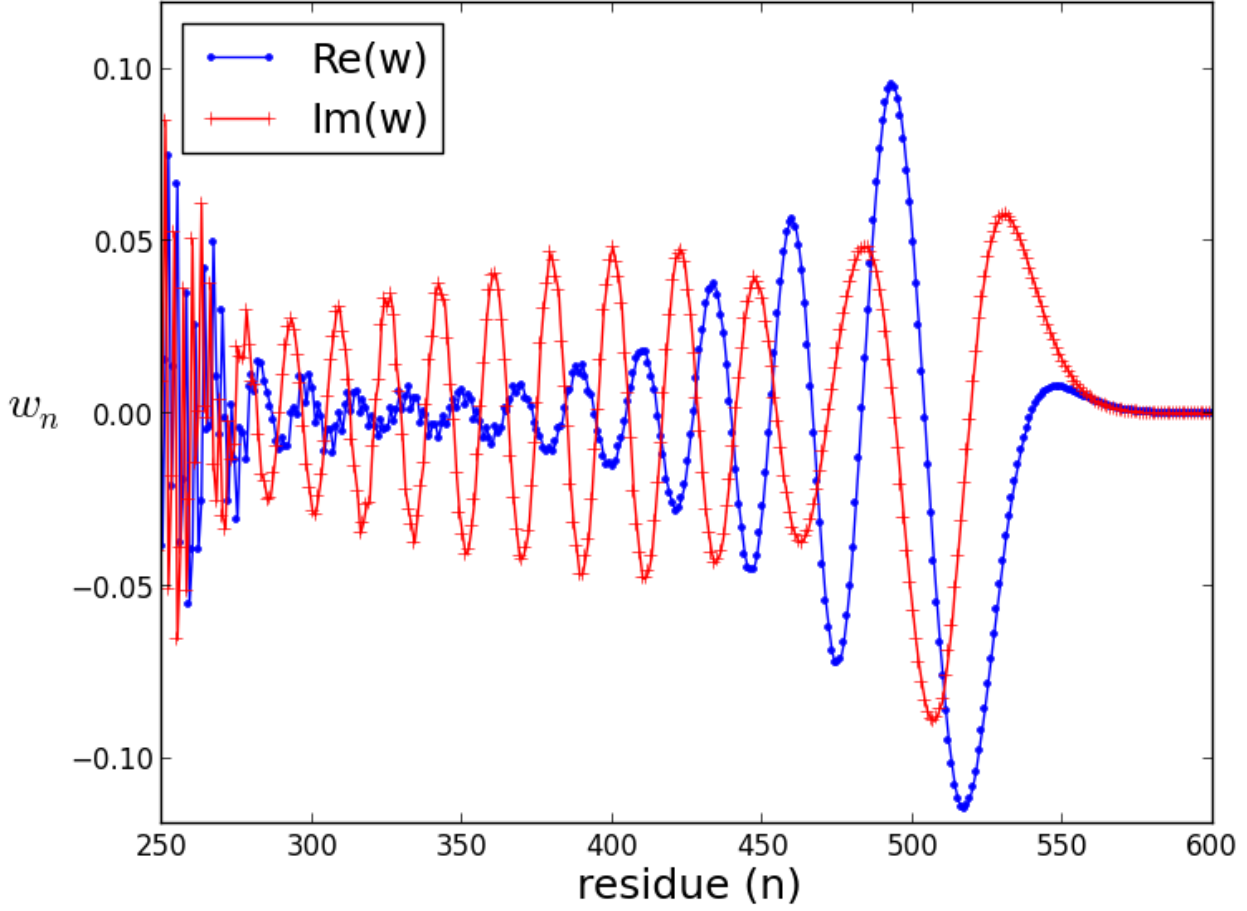$$u_\tau + u_{zzz} + \mathrm{i}\hat{\chi}|u|^2 u = 0, \tag{50}$$

FIG. 5. (Color online) Real and imaginary parts of $w_n = i^{n-1}\psi_n$ for the Davydov system with stronger nonlinear coupling $\chi = 62$, otherwise as in Fig. 4.

which is sometimes called the *third derivative nonlinear Schrödinger equation*. For either of these equations, the linearization is the Airy PDE

$$u_\tau + u_{zzz} = 0, \tag{51}$$

and the impulsive initial conditions considered here can be associated with its fundamental solution

$$u(z,\tau) = \frac{1}{(3\tau)^{(1/3)}} \mathrm{Ai}\left(\frac{z}{(3\tau)^{(1/3)}}\right). \tag{52}$$

Converting back gives approximate solutions

$$\psi_n \approx \frac{i^{n-1}}{t^{1/3}} \mathrm{Ai}\left(\frac{n - vt}{[(27\hat{J} + \hat{L})t]^{1/3}}\right), \quad v = 6\hat{J} + 2\hat{L}. \tag{53}$$

Proposals for further analysis. For the related case of discrete NLS equations of the form

$$i\frac{d\psi_n}{dt} + \psi_{n-1} + \psi_{n+1} + \chi f(\psi_{n-1}, \psi_n, \psi_{n+1}) \tag{54}$$

with cubic nonlinearities f having the gauge symmetry (14), Pelinowsky and Rothos [8] showed that solutions of the nonlinear equation for small χ bifurcate from solutions of the linearization at certain points, in particular the
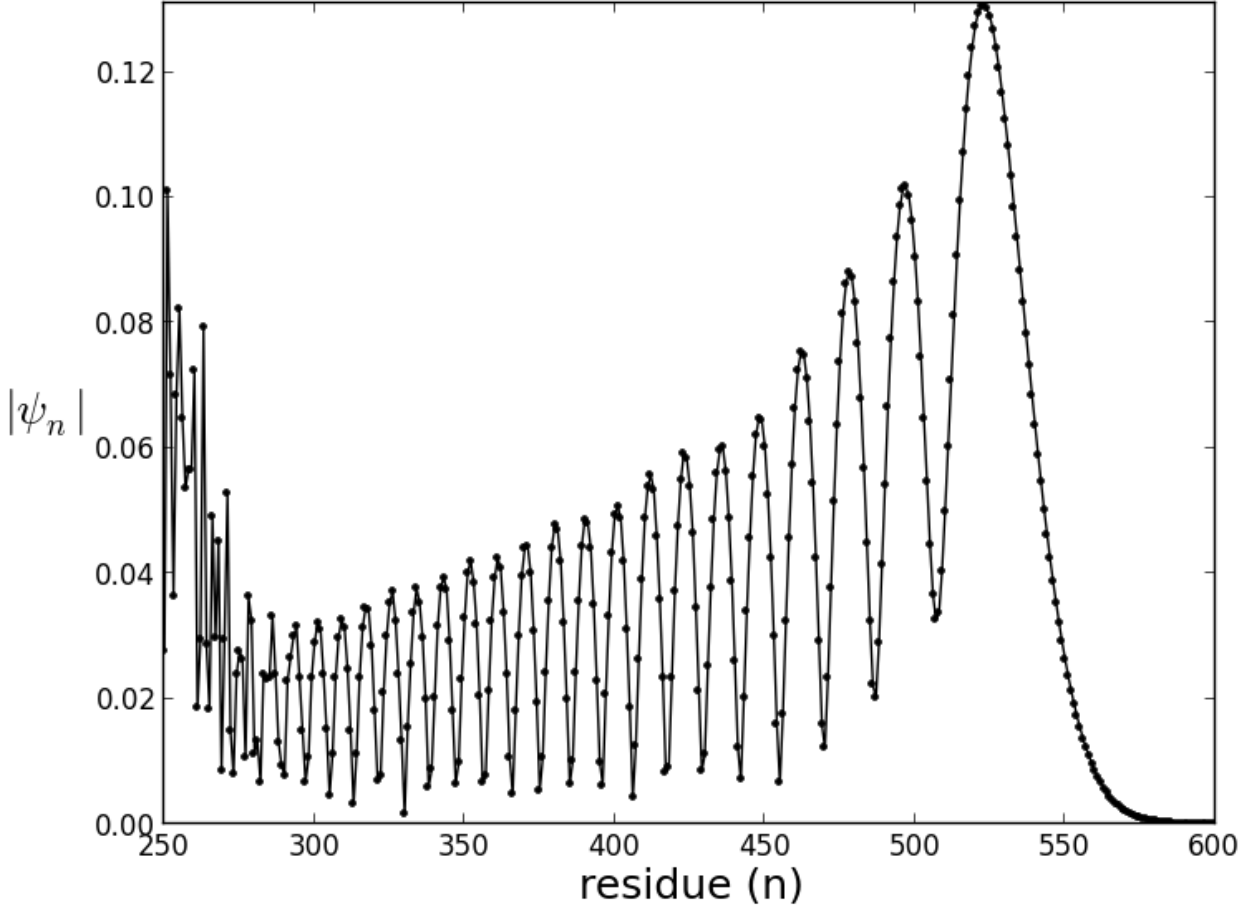
FIG. 6. $|\psi_n|$ for the Harmonic Davydov-Scott system ($\gamma = 0$): otherwise as in Fig. 2. Note the close similarity to that figure, showing that the added anharmonic force term has little significance.

one $k = -\pi/2$, $\omega = 0$ seen above. It seems likely that a similar analysis would apply here. Beyond that, what the numerical results suggest, and which should be analyzed further, is that the nonlinearity provides some "dispersion management", preventing the leading pulse from spreading as fast as in the linearization, and making it more dominant compared to the following oscillation train.

VI. CONCLUSIONS

1. The sustained traveling exciton pulses seen in Davydov-style exciton-phonon models of energy propagation in α-helix protein are well approximated by the subsonic, small mass approximation, giving a variant of the discrete NLS equation.

2. As noted by other authors, the main part of the pulse has magnitude $|\psi_n|$ that varies slowly, suggesting a long wave PDE approximation. However, the phase of the ψ_n varies rapidly in index n, by about a quarter turn at each step, and thus the slow spatial variation is instead in $w_n = i^{n-1}\psi_n$. This leads to a PDE approximation by the third derivative nonlinear Schrödinger equation $w_\tau + w_{zzz} = i|w|^2 w$, which indeed gives solutions fitting well to the fastest moving part of the solutions.

3. Linearization of this to the Airy PDE $w_\tau + w_{zzz} = 0$ also gives a good qualitative fit to many features such as pulse speed, with the main nonlinear deviation being in the most intense front-most part of the pulse.
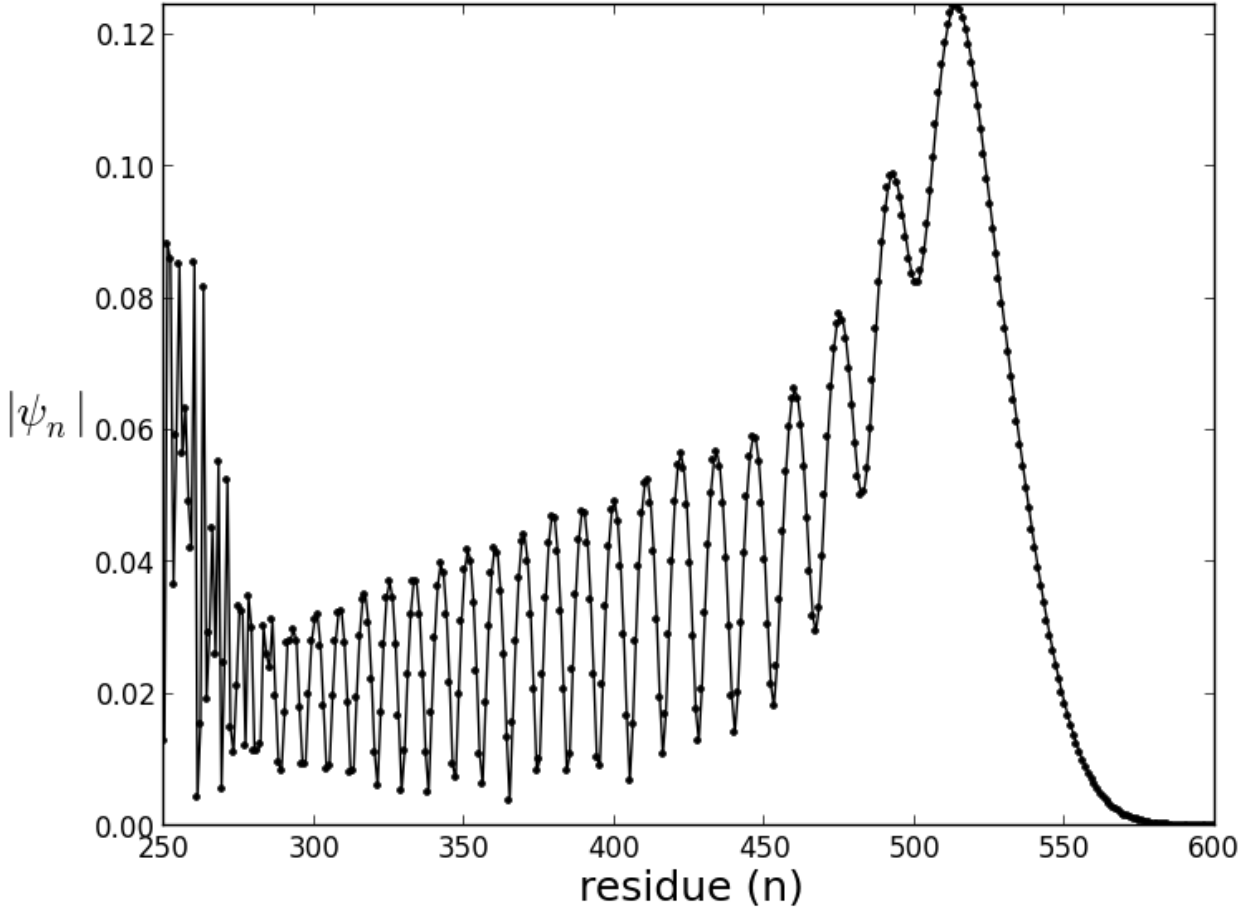
FIG. 7. $|\psi_n|$ for the Harmonic Davydov-Scott system with stronger nonlinear coupling $\chi = 62$, otherwise as in Fig. 6. Note the close similarity to Fig. 3, showing again that an anharmonic correct to the force has little significance.

4. Analysis of the linearized discrete system also explains a good part of the observed behavior: it is not nearly as accurate as the above nonlinear PDE in describing the leading part of the pulse, but explains the second, slower pulse for which the PDE is not applicable.

5. Evidence of nonlinear "self-trapping" effects are seen, in that the leading hump of the pulse remains stronger and narrower as time increases than those of the linearization, supporting more sustained propagation than a linear model would predict.

6. The higher order exactly energy-momentum conserving time-discretization method used is seen to handle well the stiffness that can arise in such systems, making it a good candidate for similar problems, including spatial discretization of various stiff nonlinear dispersive PDE's.

[1] A. S. Davydov, *Theory of Molecular Excitations* (Plenum press, New York, 1971).
[2] A. S. Davydov and N. I. Kislukha, Phys. Status Solidi B **59**, 465 (1973).
[3] A. S. Davydov, Physica Scripta **20**, 387 (1979).
[4] A. C. Scott, Physica Scripta **29**, 279 (1984).
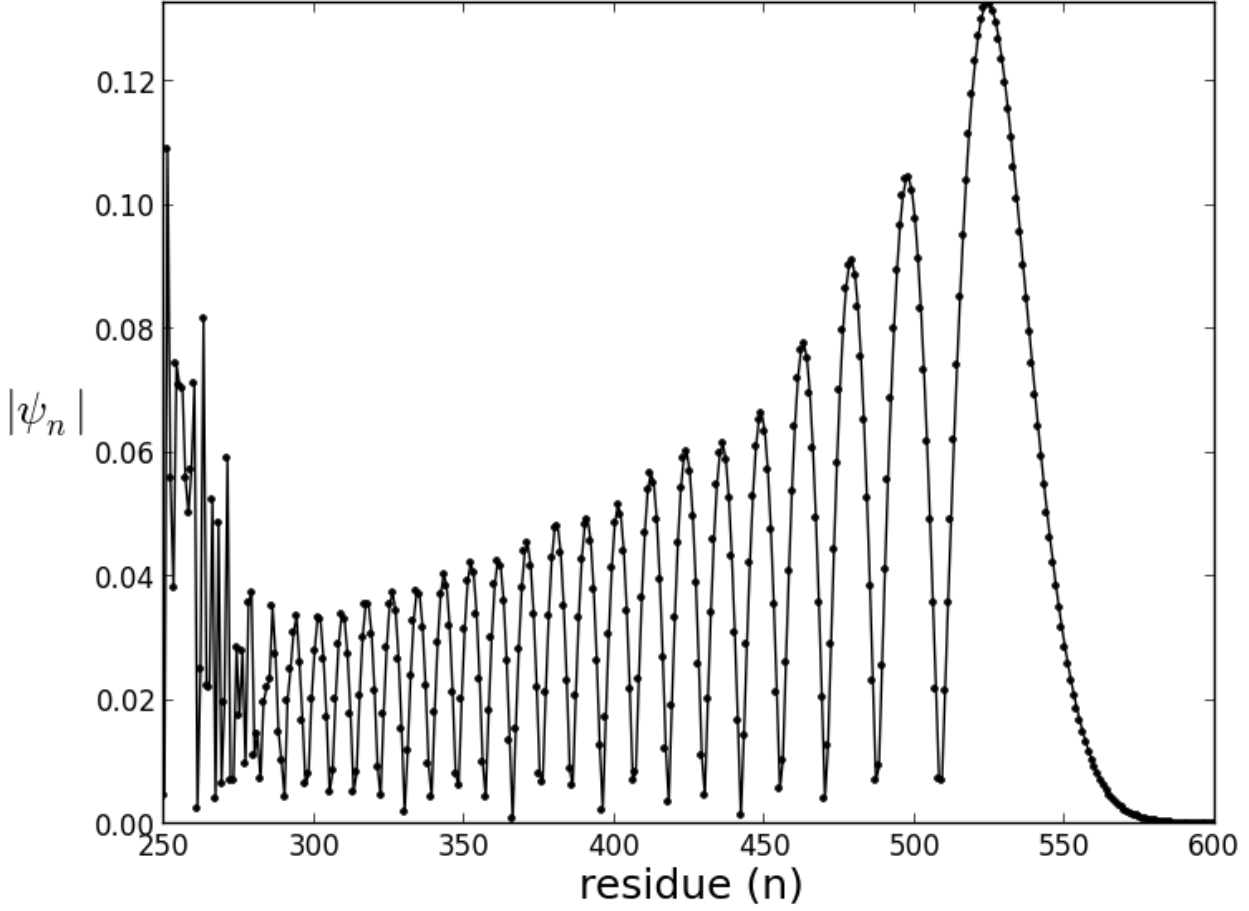[5] A. S. Davydov and A. V. Zolotariuk, Phys. Stat. Sol. (b) **115**, 115 (1983).

FIG. 8. $|\psi_n|$ at $t = 40$ for the linearization $\chi = 0$. Note the broad similarity to Fig. 2.

[6] A. S. Davydov and A. V. Zolotariuk, Physica Scripta **30**, 426 (1984).
[7] L. Brizhik, A. Eremko, L. Cruzeiro-Hansson, and Y. Olkhovska, Physical Review B **61**, 1129 (2000).
[8] D. Pelinovsky and V. Rothos, Physica D **202**, 16 (2005).
[9] V. A. Kuprievich and V. Kudritskaya, Preprint ITP-82-64E (Institute for Theoretical Physics, Kiev, 1982).
[10] H. Freedman, P. Martel, and L. Cruzeiro, Phys. Rev. B **82**, 174308 (2010).
[11] A. C. Scott, Physica Scripta **25**, 651 (1982).
[12] E. Hairer, C. Lubich, and G. Wanner, *Geometric Numerical Integration: Structure Preserving Algorithms for Ordinary Differential Equations*, 2nd ed. (Springer, 2006).
[13] O. Gonzales, Journal of Nonlinear Science **6**, 449 (1996).
[14] O. Gonzales and J. C. Simo, Comput. Methods Appl. Mech. Eng. **134**, 197 (1996).
[15] B. LeMesurier, Mathematics and Computers in Simulation **82**, 1239 (2012), published online 30 December 2010.
[16] B. LeMesurier, Physica D **241**, 1 (2012), published online 1 Oct 2011.
[17] M. Creutz and A. Gocksch, Phys. Rev. Lett. **63**, 9 (1989).
[18] E. Forest, AIP Conference Proceedings **184**, 1106 (1989).
[19] M. Suzuki, Phys. Lett. A **135**, 319 (1990).
[20] H. Yoshida, Phys. Lett. A **150**, 262 (1990).
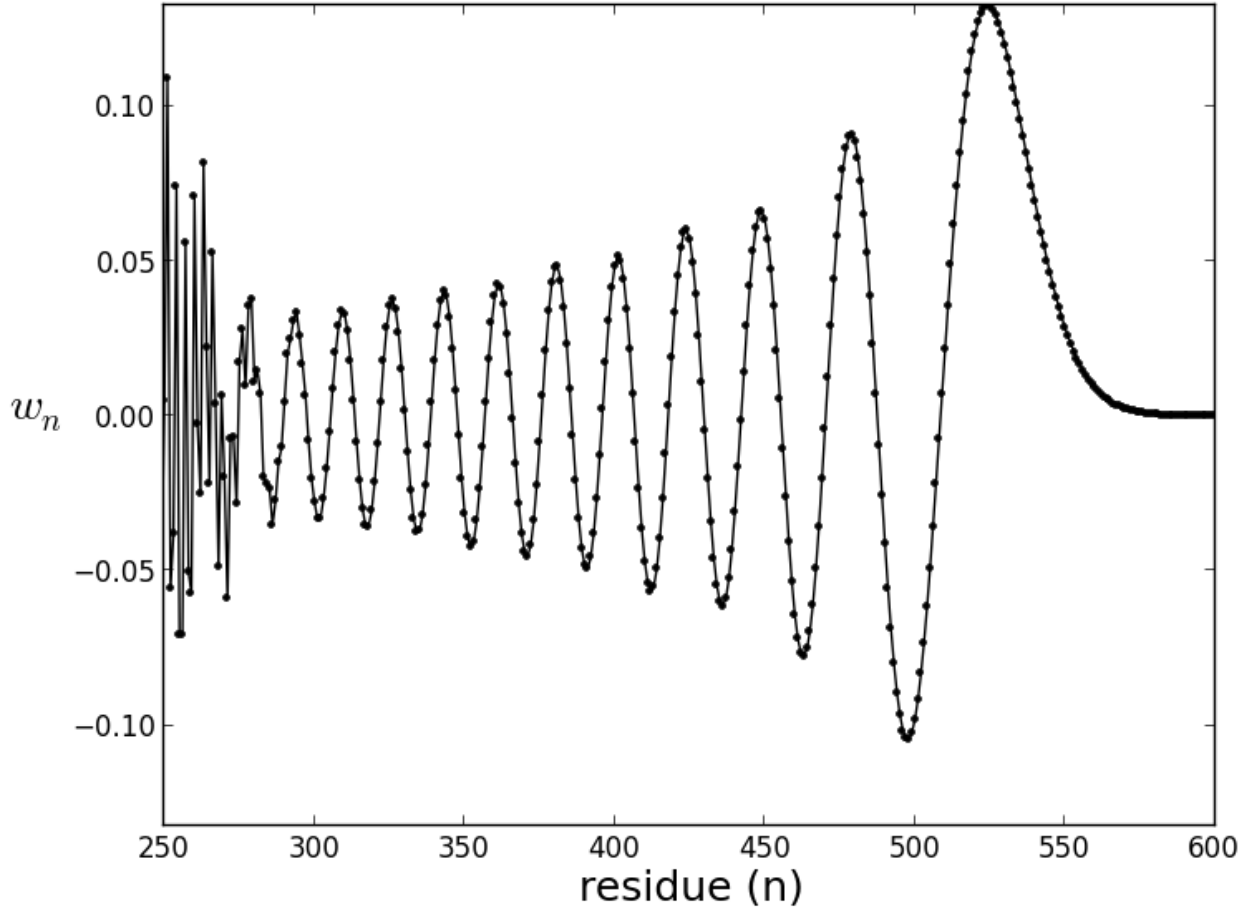[21] Z. Ge and J. E. Marsden, Phys. Lett. A **133**, 134 (1988).

FIG. 9. $w_n = \mathrm{i}^{n-1}\psi_n$, which is now real-valued, for the linearization $\chi = 0$. Compare to both Fig. 4 and the Airy function.